ISSN 0036-0236, Russian Journal of Inorganic Chemistry, 2013, Vol. 58, No. 3, pp. 259–264. © Pleiades Publishing, Ltd., 2013.
Original Russian Text © E.S. Buyanova, M.V. Morozova, Yu.V. Emel'yanova, S.A. Petrova, R.G. Zakharov, V.M. Zhukovskii, 2013, published in Zhurnal Neorganicheskoi Khimii, 2013, Vol. 58, No. 3, pp. 306–311.

SYNTHESIS AND PROPERTIES OF INORGANIC COMPOUNDS

Synthesis, Structure, and Conductivity of BINBVOX Ceramics

E. S. Buyanova[a], M. V. Morozova[a], Yu. V. Emel'yanova[a], S. A. Petrova[b], R. G. Zakharov[b], and V. M. Zhukovskii[a]

[a] *Ural Federal University named after the first President of Russia B.N. Yeltsin, ul. Mira, 19, Yekaterinburg, 620002 Russia*
[b] *Institute of Metallurgy, Ural Branch, Russian Academy of Sciences, ul. Amundsena 101, Yekaterinburg, 620016 Russia*

Received November 15, 2011

Abstract—The preparation and the structure and transport characteristics of $Bi_4V_{2-x}Nb_xO_{11}$ (BINBVOX) were studied. A comparative analysis of the synthesis of solid solutions was performed. The sintering of ceramics and the electrical conductivity as a function of temperature, composition and partial oxygen pressure were studied.

DOI: 10.1134/S0036023613030030

Solid solutions based on $Bi_4V_2O_{11}$, where vanadium is partially replaced by another cation (ME), form a BIMEVOX family, which is characterized by high oxygen ionic conductivity at moderate temperatures. According to Abraham et al. [1], bismuth vanadate contains the layers of $(Bi_2O_2)^{2+}$, which alternate with the layers of $(VO_3\square_{0.5})^{2-}$ having anionic sublattice vacancies (□). The $Bi_4V_2O_{11}$ compound undergoes a number of polymorphic transformations: $\alpha \xrightarrow{720\,K} \beta \xrightarrow{840\,K} \gamma$. The high-temperature γ modification possesses the highest conductivity. The tetragonal structure of γ-$Bi_4V_2O_{11}$ contains three nonequivalent oxygen positions: O(1) in the layer of Bi_2O_2, apical position O(2), and position O(3) in the base plane of V–O polyhedrons. The structure exhibits a maximum disorder of oxygen atoms on positions O(2) and O(3) [2].

A number of publications were dedicated to studies of niobium-substituted bismuth vanadates. According to published data [3], the composition $Bi_2V_{1-x}Nb_xO_{5.5}$ (BINBVOX) occurs in α-, β-, and γ modifications at $0 < x \le 0.075$, $0.075 < x \le 0.15$, and $0.15 < x \le 0.30$, respectively. Steil et al. [4] found that the thermal stability of BIMEVOX membranes, where a high-valence metal is a dopant ($Bi_2V_{0.75}Nb_{0.25}O_{5.5}$ or BINBVOX.25), is much higher than that of other compositions. At small dopant concentrations, the composition $Bi_2V_{0.95}Nb_{0.05}O_{5.5}$ crystallizes in an orthorhombic α modification at room temperature [5]. A long exposure (200 h at 873 K) leads to the partial decomposition of a solid solution and the appearance of $BiVO_4$ and $Bi_{3.5}V_{1.2}O_{8.25}$ impurity phases. The temperature dependence of the electrical conductivity of $Bi_2V_{0.95}Nb_{0.05}O_{5.5}$ exhibits inflections corresponding to the $\gamma \to \beta \to \alpha$ phase transitions on cooling. Compounds from the BIMEVOX family are mainly prepared by classical ceramic processing; however, this method is complicated by the occurrence of multistep solid-phase reactions. As an alternative, various synthetic procedures with the use of liquid precursors were proposed. At the first stage, a mixture of necessary components in a dissolved state is obtained. Next, insoluble salts can be coprecipitated; a colloidal solution can be prepared (sol–gel method); a complex-forming agent, a polymer, and a reducing or oxidizing agent can be introduced; then, the thermal treatment of the resulting precursor can be performed. Finely dispersed BIFEVOX [6], BITIVOX [7], and BICOVOX [8] powders were prepared in this manner. Attempts at preparing a $Bi_2VO_{5.5}$ phase and BIMEVOX (ME = Zn, Sc, Sb, In, and Pb) by mechanochemical synthesis have been made [9, 10]. Diffraction patterns characteristic of the high-temperature γ phase were obtained for BIMEVOX. On the contrary, a mixture of phases with the structures of fluorite and clinobisvanite was detected in the composition of ($2Bi_2O_3 + V_2O_5$), which ideally corresponds to the Aurivillius phase formula $Bi_2VO_{5.5}$. According to Zyryanov [9], compounds with incongruent melting, including $Bi_2VO_{5.5}$, are not formed upon mechanical synthesis. However, Castro et al. [10] managed to stabilize γ-$Bi_4V_2O_{11}$ by a mechanochemical activation method followed by annealing at a moderate temperature without the introduction of iso- or heterovalent substituents into the positions of V.

This work was dedicated to a study of the preparation, structure, and electrical conductivity of $Bi_4V_{2-x}Nb_xO_{11}$ solid solutions.

EXPERIMENTAL

A standard ceramic processing in a temperature range of 770–1070 K, a coprecipitation method, and mechanochemical activation were used for the synthesis of $Bi_4V_{2-x}Nb_xO_{11}$. Solid-phase and mechanochemical syntheses from Bi_2O_3, V_2O_5, and Nb_2O_5 oxides were carried out. An AGO-2 planetary mill under conditions with the centrifugal factor $g = 60$ and

Changes in the phase composition of solid solutions depending on temperature and exposure time

τ, min	Composition
0.5	Bi_2O_3 $Bi_{12}Nb_{0.29}O_{18.7+x}$ Bi_3NbO_7 $Bi_8Nb_{18}O_{57}$ $V_2Nb_{23}O_{62}$
2	$Bi_4V_{1.4}Nb_{0.6}O_{11}$
4	$Bi_4V_{1.4}Nb_{0.6}O_{11}$
6	$Bi_4V_{1.4}Nb_{0.6}O_{11}$
13	$Bi_4V_{1.4}Nb_{0.6}O_{11}$
23	$Bi_4V_{1.4}Nb_{0.6}O_{11}$
Annealing at 873 K	γ-Modification of $Bi_4V_{1.4}Nb_{0.6}O_{11}$

a maximum exposure time of 23 min was used for the mechanical treatment of oxides. For the preparation of $Bi_4V_{2-x}Nb_xO_{11}$ by the coprecipitation method, the solutions of bismuth nitrate $Bi(NO_3)_3$ and ammonium metavanadate NH_4VO_3 with necessary concentrations were prepared by dissolving the salts in water with the addition of concentrated HNO_3. Niobium as pentabutoxyniobium ($C_{20}H_{45}O_5Nb$) was introduced; the contents were thoroughly stirred, and NH_4OH was added to pH 9–10. The precipitate was settled for 30 min, dried at 470 K, and finally thermally treated at 1020 and 1100 K for 4–5 h.

Phase composition was monitored by X-ray diffraction (XRD) analysis (DRON-3 diffractometer; CuK_α radiation; and pyrolytic graphite monochromator on a reflected beam). Precision high-temperature XRD analysis was performed on a D8 ADVANCE diffractometer (CuK_α radiation; β filter; VÅNTEC position-sensitive detector; and Anton Paar HTK 1200N high-temperature chamber).

The TOPAS [11] and LMGP [12] program packages were used to calculate unit cell parameters.

The sizes of particles were determined with the use of a SALD-7101 Shimadzu dispersion analyzer.

Microscopic examinations were carried out with the use of a JEOL JSM 6390LA scanning electron microscope.

Dilatometric analysis was performed with the aid of a DIL 402 C Netzsch dilatometer at a heating rate of 2 K/min in a temperature range of 290–920 K; differential thermal analysis (DTA) was performed with the use of an STA 409 PC Luxx Netzsch thermal analyzer in a temperature range of 293–973 K. Aluminum oxide was used as a standard substance. The electrical conductivity of the samples was studied by impedance spectroscopy (Elins Z-2000 and Elins Z-350M impedance meters) in a temperature range of 1070–470 K and a partial oxygen pressure range of 0.21–10^{-6} [bar].

RESULTS AND DISCUSSION

A comparative analysis of the synthesis of $Bi_4V_{2-x}Nb_xO_{11}$ solid solutions by the proposed methods was performed with the use of XRD analysis. In the cases of solution (coprecipitation) and solid-phase syntheses, the powders obtained after the evaporation of initial mixtures and after each particular stage of annealing were analyzed. To determine the mechanism of the mechanochemical synthesis of BINBVOX, we analyzed diffraction patterns after mechanical treatment at specified time intervals and after final annealing at 870 K.

The processes of BINBVOX formation in the coprecipitation synthesis are analogous to phase formation processes in the solid-phase synthesis. The X-ray diffraction patterns of primary amorphized powders obtained at 470 K in a drying process exhibited weak reflections due to $Bi_4V_{2-x}Nb_xO_{11}$. This fact suggests that the BINBVOX solid solution begins to form at the stage of the pyrolysis of initial precursors. The DTA curves exhibit thermal effects accompanied by weight changes. On the average, the weight change is 5–15%, and, as well as thermal effects, it depends on decomposition and the removal of organic residues and metal nitrates. The thermal decomposition of precursors is complete at 803–823 K.

The X-ray diffraction patterns of the samples annealed at 823–873 K exhibit all of the main reflections of $Bi_4V_{2-x}Nb_xO_{11}$; these temperatures are 50–100 K lower that those of the solid-phase synthesis. The formation of solid solutions always proceeds through the step of the formation of the $BiVO_4$ vanadate. In the coprecipitation method, Bi_2O_3, Nb_2O_5, and $Bi_8Nb_{18}O_{57}$ were detected as intermediate products. The same set of phases was also detected in the solid-phase synthesis. The formation of solid solutions with the use of liquid precursors was complete at 1023 K or, in the case of the solid-phase synthesis, at 1073–1103 K. Phase formation on mechanical activation (see the table) was significantly different. Initially, a mixture of a large number of phases was formed; however, the $Bi_4V_{2-x}Nb_xO_{11}$ solid solution was completely formed after a 2-min exposure. The final product after mechanical treatment and two-hour annealing at 873 K was the γ modification of the solid solution.

Thus, the $Bi_4V_{2-x}Nb_xO_{11}$ solid solutions were prepared by different methods in the region of substituent concentrations $x \le 0.9$, which is substantially wider than that in previous studies [3, 4]. In the case of synthesis by coprecipitation (a maximum synthesis temperature of 1023 K) at a low niobium content of $x \le 0.20$, the solid solutions were formed in a monoclinic α modification (space group $C2/m$). In the region of compositions $0.2 < x < 0.4$ under the same synthesis conditions, the formation of an orthorhombic β modification with doubled parameter a came into play; therefore, the X-ray diffraction patterns exhibited the reflections of both of the modifications. Then, only a

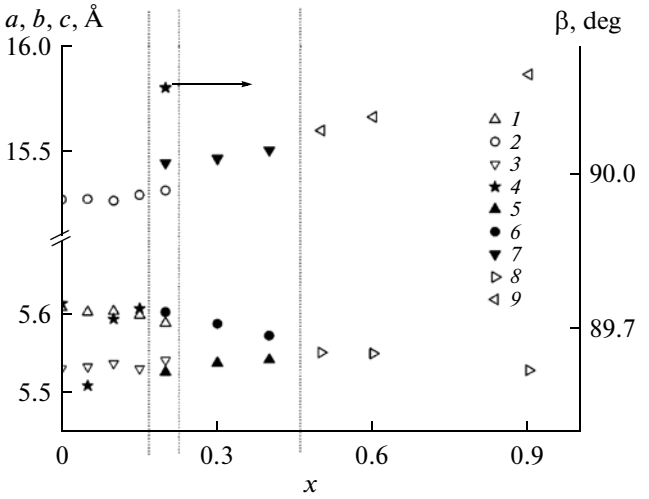

Fig. 1. Dependence of unit cell parameters on composition for $Bi_4V_{2-x}Nb_xO_{11-\delta}$ synthesized by the solid-phase method: (*1*) a_m, (*2*) b_m, (*3*) $c_m^* = c_m/3$, (*4*) β, (*5*) a_o, (*6*) b_o, (*7*) c_o, (*8*) $a_t^* = a_t\sqrt{2}$,, and (*9*) c_t.

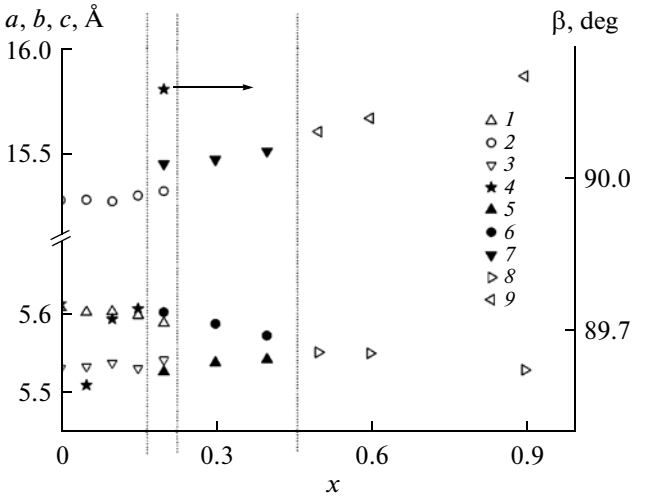

Fig. 2. Dependence of unit cell parameters on composition for $Bi_4V_{2-x}Nb_xO_{11-\delta}$ synthesized by the coprecipitation method: (*1*) a_m, (*2*) b_m, (*3*) $c_m^* = c_m/3$, (*4*) β, (*5*) a_o, (*6*) b_o, (*7*) c_o, (*8*) $a_t^* = a_t\sqrt{2}$,, and (*9*) c_t.

tetragonal γ modification was formed at $x \geq 0.5$. It is likely that the behavior was somewhat different in the solid-phase synthesis because of an increase in the final synthesis temperature to 1073 K. To $x = 0.30$, a mixture of monoclinic and orthorhombic (without the doubling of parameters) modifications was formed. In the region of $0.3 < x < 0.4$, a structural rearrangement and the formation of a mixture of orthorhombic and tetragonal phases occurred. In the solid-phase and mechanochemical synthesis, the high-temperature γ modification of $Bi_4V_{2-x}Nb_xO_{11}$ (space group *I*4/*mmm*) was unambiguously formed in the concentration range of $0.4 \leq x \leq 0.9$. With the use of a niobium-containing organic reagent ($C_{20}H_{45}O_5Nb$), a problem of stoichiometry appeared at high values of *x*. It is likely that the niobium-containing component can be partially released into a gas phase upon the thermal treatment of precursors to cause the contamination of the end product by an impurity of the bismuth vanadate $Bi_8V_2O_{17}$. Figures 1 and 2 show the dependence of the unit cell parameters of the $Bi_4V_{2-x}Nb_xO_{11}$ solid solution synthesized by solid-phase and solution methods on the composition and indicate the regions of existence of different modifications.

The estimation of the particle sizes of powders obtained by different methods the aid of laser light scattering showed that the average grain size of the powders lies in the range of 1–5 μm; however, the fraction of smaller particles (<2 μm) is greater for the samples prepared by the coprecipitation method (Fig. 3). The use of electron microscopy leads to analogous results. As can be seen in Fig. 4, in addition, the particles of powder are well agglomerated with one another to form aggregates of sizes from 1 μm.

The sintering of the $Bi_4V_{2-x}Nb_xO_{11}$ ceramics was studied by dilatometric analysis under nonisothermic conditions. Briquettes for this study were prepared with the use of a 10% solution of PVA. The process of sample sintering occurs in the same manner regardless of the composition and polymorphous modification of solid solution. The burning of the binding agent occurs at a temperature of ~500 K. Further heating leads to the thermal expansion of the sample, which is accompanied by a phase transition for the solid solutions certified as the α modification at room temperature. The most intense sintering occurs in the range of 800–1000 K. The samples with the γ-modification structure do not undergo polymorphous transforma-

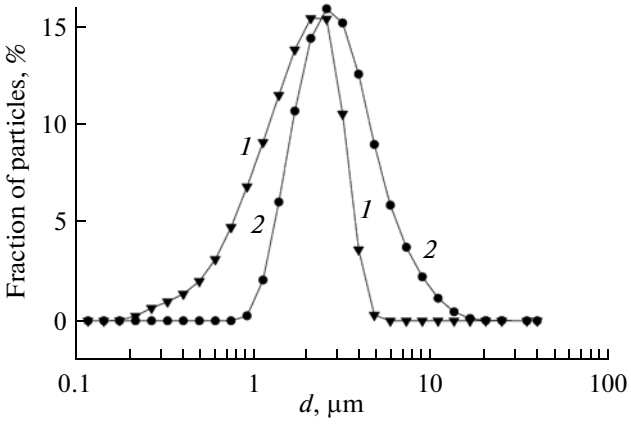

Fig. 3. Differential particle size distribution curves for $Bi_4V_{1.4}Nb_{0.6}O_{11}$: (*1*) coprecipitation and (*2*) solid-phase synthesis.

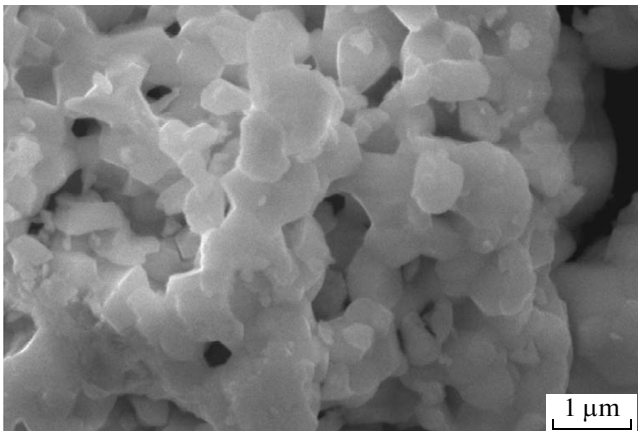

Fig. 4. Micrograph of $Bi_4V_{1.4}Nb_{0.6}O_{11}$ powder (coprecipitation method).

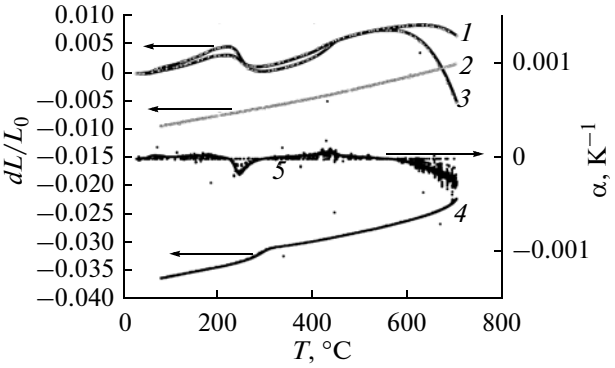

Fig. 5. Dilatometric curves of the nonisothermal sintering of BINBVOX: changes in the linear dimensions of $Bi_4V_{1.6}Nb_{0.4}O_{11}$ on (*1*) heating and (*2*) cooling; changes in the linear dimensions of $Bi_4V_{1.9}Nb_{0.1}O_{11}$ on (*3*) heating and (*4*) cooling; and the differential curve of the sintering of $Bi_4V_{1.9}Nb_{0.1}O_{11}$.

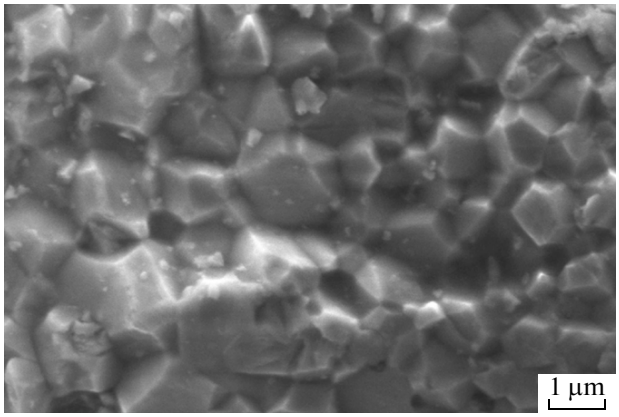

Fig. 6. Surface micrograph of a briquette of $Bi_4V_{1.1}Nb_{0.9}O_{11}$.

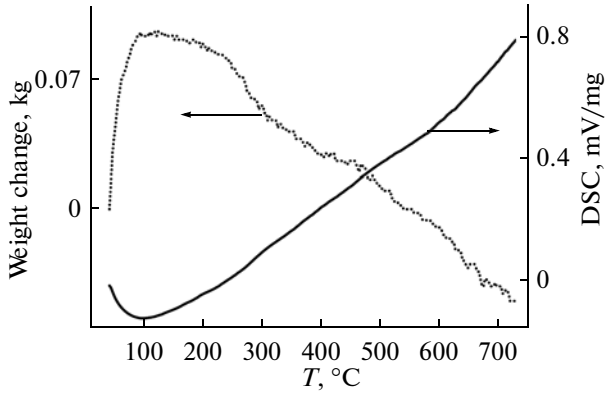

Fig. 7. Results of the TG/DSC study of $Bi_4V_{1.1}Nb_{0.9}O_{11}$.

tions on cooling (for example, BINBVOX, $x = 0.4$), but the cooling curve of a sample with $x = 0.1$ exhibit a phase transition from γ to α modification at 573 K (Fig. 5). Figure 6 shows a micrograph of the surface of a sintered briquette of $Bi_4V_{1.1}Nb_{0.9}O_{11,}$ which was obtained from powder prepared by the coprecipitation method. Well-formed crystallites and the absence of pores and cracks are noticeable. The density of the sintered briquettes is no lower than 90%. The coefficient of linear thermal expansion for the BINBVOX series is $15–21 \times 10^{-6}$ K^{-1} (820–1020 K), and it regularly decreases with dopant concentration.

The absence of phase transitions from BINBVOX compositions, which were certified as the γ modification at room temperature, under temperature changes was also confirmed by high-temperature X-ray studies and TG DSC. For example, Fig. 7 shows TG and DSC curves, and Fig. 8 shows changes in the crystal lattice parameters with temperature for the sample of the composition $Bi_4V_{1.1}Nb_{0.9}O_{11}$. In the measurements of X-ray diffraction patterns, the heating and cooling were performed at a rate of 0.5 K/s at regular intervals of 10 K. The heating and cooling were performed at $\log P_{O_2} = -0.67$ and −2 [bar], respectively. The crystal lattice parameters changed as a linear function of temperature, and a difference between parameters at different partial oxygen pressures can be due to the interaction of the sample with residual atmospheric oxygen because of the presence of defects in the oxygen sublattice. The spread of points observed under a change in the temperature is somewhat greater than the limits of determination error in a lattice parameter. This is most likely caused by tetragonal cell distortions, which manifest themselves in line broadening in the X-ray diffraction patterns, as the temperature is increased. Upon the annealing of the samples with $x = 0.5–0.9$ at 1103 K, the half-widths of reflections from the planes (006), (015), and (118/019) were greater than the others.

The electrical conductivity of BINBVOX was studied by impedance spectroscopy. Figure 9 shows typical impedance diagrams for the BINBVOX solid solutions. The impedance diagrams are characteristic of

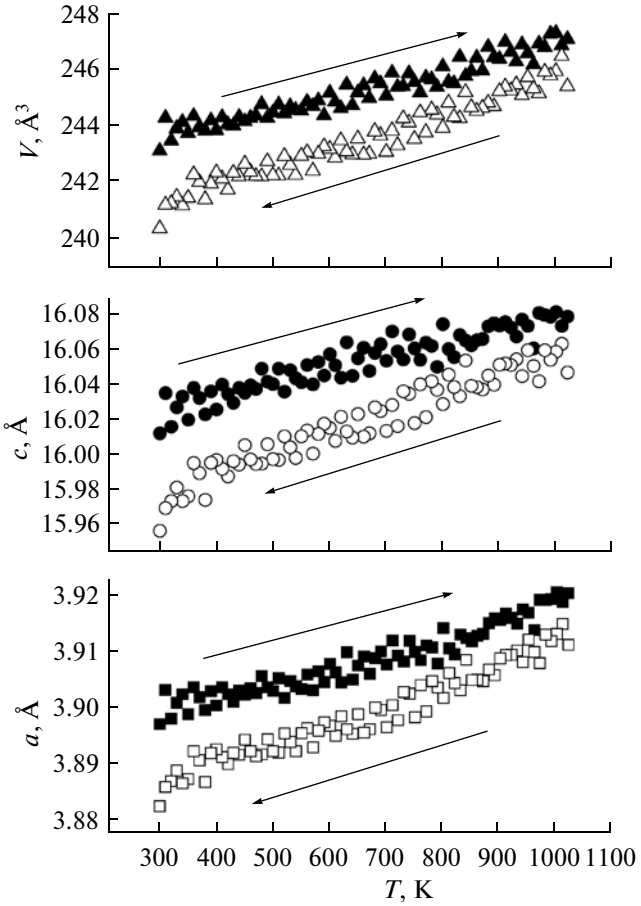

Fig. 8. Unit cell parameters of $Bi_4V_{1.1}Nb_{0.9}O_{11}$: solid and open points refer to heating at $\log P_{O_2} = -0.67$ [bar] and cooling at $\log P_{O_2} = -2$ [bar], respectively.

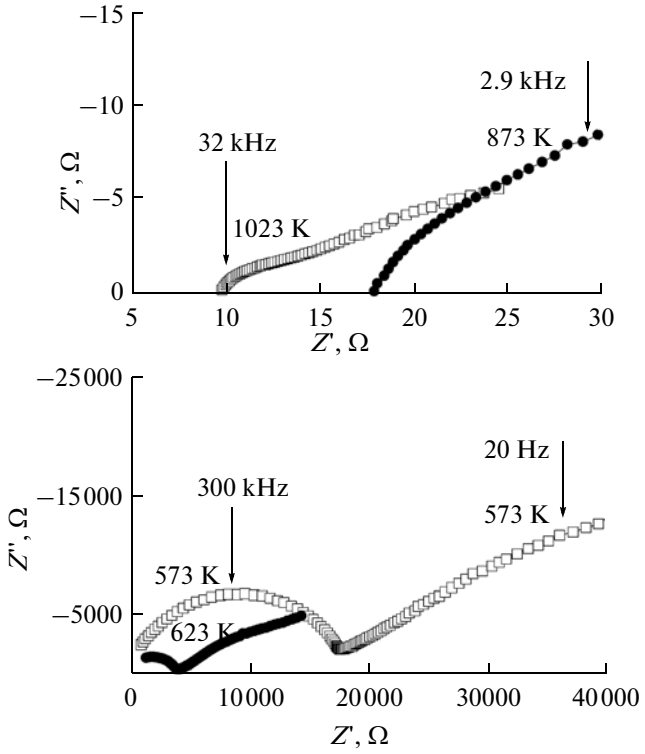

Fig. 9. Typical impedance diagrams exemplified for $Bi_4V_{1.8}Nb_{0.2}O_{11}$.

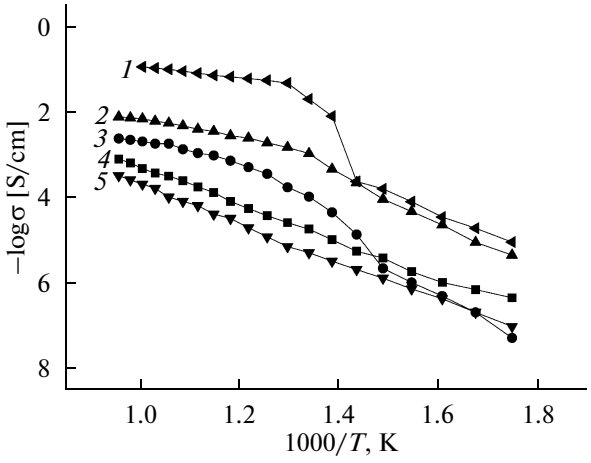

Fig. 10. Conductivity polytherms for BINBVOX: solid-phase synthesis, (*1*) $x = 0.1$, (*3*) $x = 0.2$, and (*5*) $x = 0.8$; coprecipitation method, (*2*) $x = 0.2$ and (*4*) $x = 0.8$.

ionic conductors of the BIMEVOX family, and they have a shape of two combined semicircles [6, 13–15]. They were treated with the use of equivalent circuits proposed previously [15]. Figure 10 shows the resulting conductivity polytherms for some compositions synthesized by different methods. At small dopant concentrations (for example, $x = 0.1$), the dependences exhibited a sharp inflection in a temperature range of 750–700 K, which corresponds to the direct $\gamma \leftrightarrow \alpha$ phase transition; this is consistent with structural and thermal studies. The samples from the γ-modification region exhibit an inflection, which characterizes a transition to the γ' modification on cooling, in the plot. The conductivity of the samples prepared by the coprecipitation method is higher than that of the samples obtained by the solid-phase method. An analogous behavior is also characteristic of other BIMEVOX materials [6]. The maximum values of conductivity are characteristic of small dopant concentrations ($x < 0.3$); this reflects the general tendency typical of BIMEVOX. As found previously [16], an increase in the conductivity upon the homovalent substitution of niobium for vanadium can be related to the local strengthening of Nb–O bonds in the first coordination sphere of the niobium atom, as compared with the V–O bonds, and to the small weakening of V–O(2) interactions, as compared with unsubstituted γ-$Bi_4V_2O_{11}$. In other words, the introduction of niobium into the structure of γ-$Bi_4V_2O_{11}$ leads to an

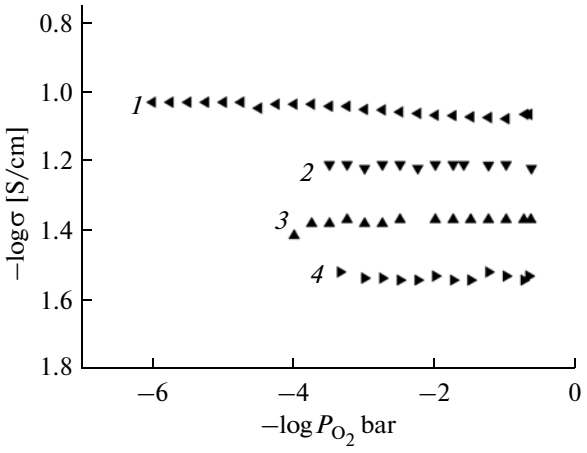

Fig. 11. Dependence of the total electrical conductivity of $Bi_4V_{1.6}Nb_{0.4}O_{11}$ on partial oxygen pressure at different temperatures: (*1*) 800, (*2*) 700, (*3*) 650, and (*4*) 600°C.

increase in the fraction of O(2) oxygen atoms, which participate in ion transport.

Figure 11 shows the dependence of the electrical conductivity on partial oxygen pressure at different temperatures based on the example of the $Bi_4V_{1.6}Nb_{0.4}O_{11}$ composition. In the test range of p_{O_2}, the dependence is almost linear; this fact suggests the predominant oxygen-ionic conductivity of solid solutions and is completely consistent with published data [5] on the measurement of ionic transport numbers in BIMEVOX.

ACKNOWLEDGMENTS

This work was supported by the Ministry of Education and Science of the Russian Federation within the framework of the Federal Goal-Oriented Program "Scientific and Scientific-Pedagogical Cadres of Innovation Russia" for 2009–2013 and was supported by the Ural Federal University within the framework of the development program of the Ural Federal University for young scientists.

REFERENCES

1. F. Abraham, J. Boivin, G. Mairesse, and G. Nowogrocki, Solid State Ionics **40/41**, 934 (1990).
2. G. Mairesse, P. Roussel, R. N. Vannier, et al., Solid State Sci. **5**, 851 (2003).
3. S. Lasure, C. Vernochet, R. N. Vannier, et al., Solid State Ionics **90**, 117 (1996).
4. M. C. Steil, F. Ratajczak, E. Capoen, et al., Solid State Ionics **176**, 2305 (2005).
5. Y. Taninouchi, T. Uda, T. Ichitsubo, et al., Solid State Ionics **181**, 1279 (2010).
6. E. S. Buyanova, S. A. Petrova, Yu. V. Emel'yanova, et al., Zh. Neorg. Khim. **54**, 1193 (2009).
7. C. H. Hervoches, M. C. Steil, and R. S. Muccillo, Solid State Sci. **6**, 173 (2004).
8. M. J. Godinho, P. R. Bueno, M. O. Orlandi, et al., Mater. Lett. **57**, 2540 (2003).
9. V. V. Zyryanov, Zh. Strukt. Khim. **45**, 135 (2004).
10. A. Castro, P. Millan, J. Ricote, and L. Pardo, J. Mater. Chem. **10**, 767 (2000).
11. Diffrac Plus (Topas Bruker AXS, Karlsruhe, 2006).
12. J. Laugier and B. Bochu, LMGP-Suite of Programs for the Interpretation of X-ray Experiments (ENSP Lab. Materiaux Genie Phys., Grenoble, 2003).
13. E. S. Buyanova, S. A. Petrova, Yu. V. Emel'yanova, et al., Russ. J. Inorg. Chem. **54**, 864 (2009).
14. V. M. Zhukovskii, E. S. Buyanova, Yu. V. Emel'yanova, et al., Elektrokhimiya **45**, 547 (2009).
15. E. S. Buyanova, Yu. V. Emel'yanova, M. V. Morozova, et al., Elektrokhimiya **46**, 810 (2010).
16. V. M. Zainullina, V. M. Zhukovskii, E. S. Buyanova, and Yu. V. Emel'yanova, Russ. J. Inorg. Chem. **52**, 225 (2007).